Accepted Manuscript

Title: On the thermal stabilization of carbon-supported SiO_2
catalysts by Phosphorus. Evaluation in the oxidative
dehydrogenation of ethylbenzene to styrene and a comparison
with relevant catalysts

Author: Valeriya Zarubina Hesamoddin Talebi Harrie Jansma
Kinga Góra-Marek Christian Nederlof Freek Kapteijn Michiel
Makkee Ignacio Melián-Cabrera

Please cite this article as: Valeriya Zarubina, Hesamoddin Talebi, Harrie Jansma,
Kinga Góra-Marek, Christian Nederlof, Freek Kapteijn, Michiel Makkee, Ignacio
Melián-Cabrera, On the thermal stabilization of carbon-supported SiO2 catalysts
by Phosphorus.Evaluation in the oxidative dehydrogenation of ethylbenzene to
styrene and a comparison with relevant catalysts, Applied Catalysis A, General
http://dx.doi.org/10.1016/j.apcata.2016.01.024

This is a PDF file of an unedited manuscript that has been accepted for publication.
As a service to our customers we are providing this early version of the manuscript.
The manuscript will undergo copyediting, typesetting, and review of the resulting proof
before it is published in its final form. Please note that during the production process
errors may be discovered which could affect the content, and all legal disclaimers that
apply to the journal pertain.

On the thermal stabilization of carbon-supported SiO₂ catalysts by Phosphorus. Evaluation in the oxidative dehydrogenation of ethylbenzene to styrene and a comparison with relevant catalysts.

Valeriya Zarubina,[a] Hesamoddin Talebi,[a] Harrie Jansma,[b] Kinga Góra-Marek,[c]

Christian Nederlof,[b] Freek Kapteijn,[b] Michiel Makkee,[b] Ignacio Melián-Cabrera[a,d] *

[a] Chemical Reaction Engineering, ENTEG, University of Groningen, Nijenborgh 4, 9747 AG Groningen, The Netherlands.

[b] Catalysis Engineering, Chemical Engineering Department, Faculty of Applied Sciences, Delft University of Technology, Julianalaan 136, 2628 BL Delft, The Netherlands.
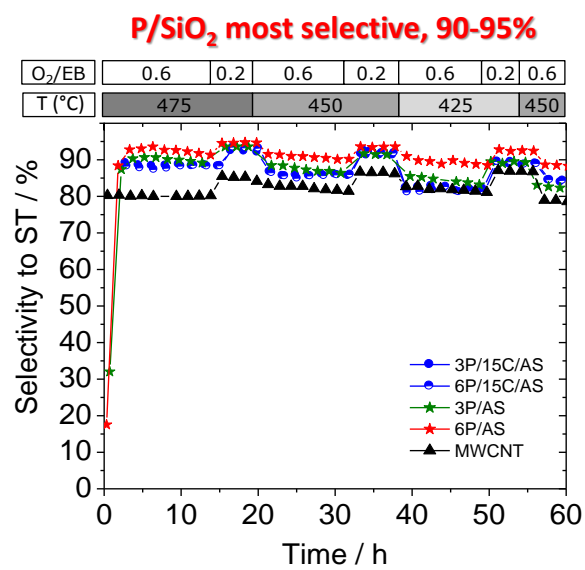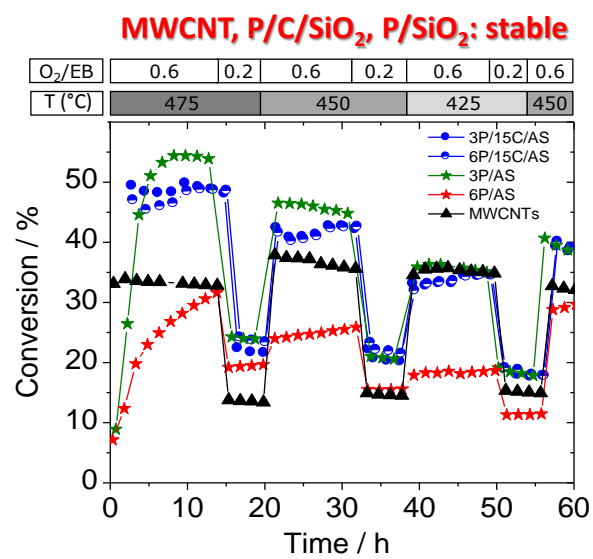
[c] Faculty of Chemistry, Jagiellonian University in Kraków, 3 Ingarden St., 30-060 Kraków, Poland.

[d] European Bioenergy Research Institute (EBRI), School of Engineering and Applied Science, Aston University, Aston Triangle, Birmingham, B4 7ET, United Kingdom.

* Corresponding Author:

i.melian-cabrera@aston.ac.uk (Ignacio V. Melián Cabrera)

Graphical abstract

Highlights

- P/C/Silica materials have been prepared by polymerization of furfuryl alcohol (FA) on a mesoporous silica, followed by H_3PO_4 addition before pyrolysis;

- P addition enhances the oxidative thermal stability of the FA-based carbon coating, based on the apparent activation energies;

- P/C/Silica materials are readily active (no induction period, as seen for P/Silica), selective and stable in the long term for the ethylbenzene oxidative dehydrogenation;

- Styrene selectivity of P/C/Silica is better than a conventional MWCNT but lower than P/Silica.

Abstract

A strategy to enhance the thermal stability of C/SiO_2 hybrids for the O_2-based oxidative dehydrogenation of ethylbenzene to styrene (ST) by P addition is proposed. The preparation consists of the polymerization of furfuryl alcohol (FA) on a mesoporous precipitated SiO_2. The polymerization is catalyzed by oxalic acid (OA) at 160 °C (FA:OA=250). Phosphorous was added as H_3PO_4 after the polymerization and before the pyrolysis that was carried out at 700 °C and will extend the overall activation procedure. Estimation of the apparent activation energies reveals that P enhances the thermal stability under air oxidation, which is a good indication for the ODH tests. Catalytic tests show that the $P/C/SiO_2$ hybrids are readily active, selective and indeed stable in the applied reactions conditions for 60 h time on stream. Coke build-up during the reaction attributed to the P-based acidity is substantial, leading to a reduction of the surface area and pore volume. The comparison with a conventional MWCNT evidences that the $P/C/SiO_2$ hybrids are more active and selective at high temperatures (450-475 °C) while the difference becomes negligible at lower temperature. However, the comparison with reference P/SiO_2 counterparts shows a very similar yield than the hybrids but more selective to ST. The benefit of the $P/C/SiO_2$ hybrid is the lack of stabilization period, which is observed for the P/SiO_2 to create an active coke overlayer. For long term operation, P/SiO_2 appears to be a better choice in terms of selectivity, which is crucial for commercialization.

4

1. Introduction

In the petrochemical industry styrene (ST) production is considered one of the major processes; styrene is used principally as a monomer for polystyrene with different grades and as a component in the synthesis of styrene-butadiene co-polymer for automobile tires. ST is industrially over 85 % produced by direct dehydrogenation of ethylbenzene (EB) over a K-promoted Fe_2O_3 catalyst at 580-630 °C using an excess of steam [1], (1):

$$EB \overset{H_2O}{\longleftrightarrow} ST + H_2 \tag{1}$$

The major feature of this process is the extremely high selectivity (>96 %), that makes the downstream processing relatively simpler, as compared to other catalytic processes. The (small) amounts of byproducts (benzene, toluene, and hydrogen) have also commercial value. The process suffers, however, from high steam consumption, moderate conversion per pass due to the equilibrium limitations, and high temperatures are required for the endothermic reaction [2]. Remarkable efforts now and in the past have been put into overcome the equilibrium recycle, reducing the operation temperature, reducing the steam to EB ratio, and replacing steam by oxidants, such as O_2 or CO_2, or combinations thereof. The use of oxidants in this process (ODH route), can in theory and will in practice reduce the reaction temperature as the equilibrium limitation disappears for the case of O_2 (2) or it is improved for the CO_2-based ODH. It is nevertheless not an easy task finding a highly selective catalyst in the presence of an oxidant. This is because EB is also gasified and/or fully oxidized into CO/CO_2 that has no economic value. Besides the selectivity, the ODH process is not commercialized yet due to the limited catalyst stability.

$$EB + \tfrac{1}{2} O_2 \rightarrow ST + H_2O \tag{2}$$

Two types of catalyst families have been proven to be active and selective for EB ODH. Inorganic-based materials such as aluminas [3-8], metal pyrophosphates [9-11], and

5

phosphates [10-20] or P-supported silica [10,21] have been reported as a first class of catalysts. There is a general consensus that the coke deposit generated on the acid sites under these oxidative reaction conditions is more active and selective for the production of ST than the inorganic material itself [3-6,8,22]. In fact, the formation of coke initially improves the activity and selectivity, however, in the long term an excess of carbon deposit leads to catalyst deactivation. Depending on the reactions conditions there is an activation period to achieve pseudo-stationary conditions, *i.e.* a period of time necessary to achieve full coverage of active coke on the surface, where the conversion and selectivity to styrene achieve both a maximum. We recently showed that for alumina it can be significantly shortened by working at 475 °C instead of 450 °C [8].

The second catalyst family includes carbon based materials, such as activated carbons [23-29], carbon nano-fibers [30-35], onion-like carbon [36,37], nanodiamonds [37-44], multiwall carbon nanotubes (MWCNT) [38,45-49], graphitic carbide [50], porous graphene [51] and graphene-based composites [43,44]. These materials are readily active and selective; the reported selectivities lie within 70-90 % that is low to moderate, as compared to the commercial steam dehydrogenation process (>96%). In some cases, the reported selectivity is significantly high, ranging 90-97%, however, in an excess of oxygen [48,52,53]. The performance and stability of these carbon-based catalytic materials is in general difficult to compare due to large differences in the applied operation conditions; principally temperature range, EB concentration, space velocity, and O_2:EB vary significantly among the reported literature. We have recently compared, under identical and relevant ODH conditions, various types of carbon-based catalysts, ranging from conventional to nano-structured carbons [54]. It was found that nano-structured MWCNT is the most stable material; the structure resists the reaction conditions showing an EB conversion of ca. 30% (but deactivating) with a steady selectivity of *ca.* 80%. On the other hand, the low-cost carbon-SiO_2 (C-SiO_2) hybrids

6

prepared by furfuryl alcohol polymerization and pyrolysis were stable only for 15h; after that, the carbon of the hybrids decomposes completely rendering the almost inactive and non-selective silica matrix.

In this work we propose a strategy to enhance the thermal stability of these C/SiO_2 hybrids for the ODH reaction. It is well-known that phosphorous has an inhibiting effect on the carbon combustion [55-59]; in this study we investigated the effect of the P addition (on two loadings) on a furfuryl alcohol based silica hybrid. The performance of these P-based hybrid catalytic materials is compared to state-of-the-art P/SiO_2 and a conventional MWCNT. The catalyst stability under the ODH reaction conditions will be evaluated from the combustion apparent activation energies.

2. Experimental methods

2.1. Materials

Bare precipitated amorphous silica extrudates (61138, denoted here as AS) was kindly supplied by Saint-Gobain NorPro, a Division of Saint-Gobain Ceramic Materials GmbH. Purified MWCNT (C>96 *wt*.% experimentally determined) was kindly supplied by Hyperion (CS-02C-063-XD). Activated carbons (denoted as AC) were supplied by Norit (ROX 0.8). For the impregnations on silica, we employed the liquid pore volume (V_{LPV}) that was experimentally determined (V_{LPV}=1.05 cm^3.g^{-1}): water was added to *ca.* 10 g of material that is repeatedly shaken after each water addition until the material turned shiny. Note that this method is different to the reported one by Innes [60]; the latter is based on the caking of the catalyst particles. Note that V_{LPV} (1.05 cm^3.g^{-1}) is larger than that of the gas adsorption value (0.842 cm^3.g^{-1}, AS in Table 1) because water fills pores larger than 100 nm. A similar V_{LPV} was assumed for the (Furfuryl Alcohol) FA/SiO$_2$ composites during the P addition.

7

2.2. Catalyst preparation

2.2.1. Preparation of the C/SiO$_2$ catalysts

Among the various carbon sources the furfuryl alcohol polymerization route [61-70] was considered since it has given successful examples of stable carbon nanoreplicas [71-73]. Commercial amorphous precipitated SiO$_2$ (AS) was used as support. The solid was pre-sieved into the 212-425 μm fraction that was obtained by crushing the commercial extrudates and sieving. The carbon precursor was added by incipient wetness impregnation of the carbon precursor using 5% extra liquid volume regarding the solid pore volume. Furfurylalcohol (FA, Acros Organics, 98%) was used as carbon precursor and oxalic acid (OA, Acros Organics, >99%) as catalyst. The support (typically 3 g) was first degassed under vacuum at 150 °C during 4 h. A carbon-precursor solution was prepared by mixing FA and OA in a molar ratio of 250 based on previous polymerization studies [73] and water. Then 3.15 mL of the FA/OA aqueous solution was added to the support to obtain a carbon loading of ~15 *wt.*%, in the final pyrolyzed hybrid, assuming that only C is present in the final composite material. The wet material was shaken (VWR, digital DVX-2500) during 4 minutes at 2500 rpm at room temperature to distribute the solution evenly. Afterwards, the FA polymerization of the samples was carried out at 160 °C in an atmospheric oven during 8 h; the sample is named 15C/AS.

2.2.2. Preparation of the P/C/SiO$_2$ catalysts

The phosphorus was added onto the dried 15C/silica material before pyrolysis as diluted orthophosphoric acid (H$_3$PO$_4$); a solution (10 mL) was prepared by mixing 0.651 mL (or 1.345 ml) of H$_3$PO$_4$ (Merck, 85%) with water; then 3.15 mL of the solution was (incipient wetness) impregnated into the 15C/AS dried material (3 g). This corresponds to a phosphorous loading of *ca.* 3 or 6 *wt.*% (as P). Afterwards, the samples were shaken during 4 min at 2500 rpm at room temperature and dried at 70 °C overnight in an

8

atmospheric oven. The catalysts are denoted as 3P/15C/AS and 6P/15C/AS.

2.2.3. Carbonization protocol

The carbonization of the C/SiO$_2$ and P/C/SiO$_2$ samples was carried out by pyrolysis in a quartz-tube housed tubular oven (Nabertherm RT 50/250-11). The sample (~3 gram) was loaded in a flat quartz crucible and placed horizontally in the centre of the heating zone of the furnace. After closing and purging the tube for 30 min with N$_2$, the sample was heated at 1 °C.min^{-1} from room temperature until 700 °C for 3 h and subsequent cooling down in a nitrogen flow of 150 mL.min^{-1} STP.

2.2.4. Preparation of the P/SiO$_2$ reference catalysts

Reference catalysts based on P on silica (3 and 6 *wt*.%) were prepared for comparison. The P addition protocol is nearly identical to that described above for the P/C/SiO$_2$ hybrid; using 212-425 μm pre-sieved AS material that was obtained by crushing the commercial extrudates. The impregnated samples were then shaken during 4 min at 2500 rpm at room temperature and dried at 70 °C overnight in an atmospheric oven. The samples were calcined in an air box furnace (Nabertherm LT9/11) from room temperature at 4 °C.min^{-1} until 500 °C and kept for 8 h. The catalysts are denoted as 3P/AS and 6P/AS. For this P/SiO$_2$ catalyst formulation, it is noted that the calcination temperature ranging 500-700 °C does not have an influence in the performance (unpublished results); a low temperature was applied. The chosen concentrations, 3 and 6 *wt*.% represents 75% and 150% of the theoretical silica's surface monolayer capacity, assuming an homogeneous P deposition and the cross section for a phosphate group to be 24 Å^2 [74]. The monolayer capacity derived from Ar physisorption at 87 K was employed, since the Ar cross section is not affected by the surface polarity.

2.3. Characterization

The total organic content of the fresh and spent catalysts was quantified by thermogravimetric analysis (TGA) on a Mettler-Toledo analyzer (TGA/SDTA851e) using a flow of synthetic air of 100 mL.min^{-1} STP. The temperature was increased from 30 to 900 °C at 10 °C.min^{-1}. Blank curve subtraction using an empty crucible was taken into account. The oxidation rate patterns (TPO) were obtained in the same instrument using the derivative of the TGA patterns.

CHN elemental analyses were carried out in a EuroVector 3000 CHNS analyzer, after dissolving the silica and the complete removal of "POx" groups (6 *wt*.% HF, 2 days at room temperature). All analyses were done in duplicate to verify possible sample heterogeneity. For these materials the standard deviation was <2%. The protocol consisted of weighing 2 mg of sample in a tin crucible using a 6-digit analytical balance (Mettler Toledo). The crucible is dropped with an autosampler into the analysis chamber and is rapidly heated at ~1000 °C, in the presence of an oxidation catalyst and oxygen. This process allows the organics to be completely decomposed into CO_2, H_2O and N_2. These gases were subsequently separated in a Porapak QS column at 80 °C and quantified with a TCD detector. Acetonitrile (99.9%) was employed as external standard.

Nitrogen physisorption analyses (–196 °C) were carried out in a Micromeritics ASAP 2020. The samples were degassed in vacuum at 250 °C for 10 h. The surface area was calculated using the standard BET method (S_{BET}) [75]. The single point gas adsorption pore volume (V_T) was estimated from the amount of gas adsorbed at a relative pressure of 0.98 in the desorption branch. The pore size distributions (PSD) were obtained from the BJH method [76], using the adsorption branch of the isotherms; the mean pore size (Φ_{BJH}) is given by the position of the PSD maximum, while the *t*-plot method [77] was

employed to quantify the micropore volume ($V\mu$) and surface area ($S\mu$), using the statistical Harkins-Jura model (3) for simplicity:

$$r(\text{Å}) = \left[\frac{13.99}{0.034 - log\left(\frac{p}{p_0}\right)}\right]^{1/2} \quad (3)$$

The apparent activation energy (AAE, E_{ACT}) of the carbon combustion was calculated by the Ozawa-Flynn-Wall model [78] using a correlation between peak temperature for a given conversion and the heating rate for four thermal analysis derivative curves:

$$\frac{d(\log \beta i)}{d(1/T_X)} \approx \text{-}0.4567 \left(\frac{E_{\text{ACT}}}{R}\right) \quad (1)$$

where β_i is heating rate (K/min) and T_X is temperature in Kelvin at iso-conversion. The TGA curves were obtained on a Mettler-Toledo analyzer (TGA/SDTA851e) using a flow of synthetic air of 100 mL.min^{-1} STP. The temperature was increased from 30 to 900 °C with a heating rate of 1, 3, 5, 10 °C.min^{-1}. Blank curve subtraction using an empty crucible was taken into account. The apparent activation energy was calculated at 80% conversion.

The concentration of both Brønsted and Lewis acid sites was determined based on quantitative in-situ IR studies with pyridine (Py) as probe molecule. FTIR spectra were recorded on a Bruker Vertex 70 equipped with a MCT-B detector and a quartz home-made IR cell having CaF_2 windows connected to a vacuum system that allows the controlled Py dosing. Around 10 mg of sample were pressed in a 1.767 cm^2 self-supporting wafer and mounted into the quartz cell. Before dosing the pyridine, the sample was preheated under vacuum ($\leq$5.10^{-6} mm Hg) at constant heating rate of 3 °C.min^{-1} up to 500 °C, maintained at this temperature for 1 h and then cooled down to 170 °C for 1 h. Pyridine gas was dosed into the sample wafer until full saturation at 170 °C. The FT-IR spectra of both the outgassed sample and upon the pyridine sorption have

been recorded at 170 °C. Spectra were measured by accumulating 100 scans at a resolution 2 cm^{-1}; the spectrum of the sample after evacuation was subtracted to each spectrum. The total concentration of Brønsted and Lewis sites was calculated using respectively the intensities of the 1545 cm^{-1} band of pyridinium ions (PyH$^+$) and the 1445 and 1455 cm^{-1} bands of coordinatively bonded pyridine to Lewis sites (PyL) by applying their respective extinction coefficients. The extinction coefficient of 0.07 and 0.1 cm^2.µmol^{-1} for the PyH$^+$ and PyL bands were applied, respectively [79]. The acid strength was determined based on pyridine thermodesorption studies. In the Py experiments, the conservation of the Py bonded to Lewis, Py-L (1445 cm^{-1}), and Brønsted, PyH$^+$ (1545 cm^{-1}), acid sites band under the desorption procedure at elevated temperature (400 °C) were taken as a measure of the acid strength of the acid sites. The ratio A_{400}/A_{170}, with A_{400} and A_{170} being the absorbance intensities of the PyH$^+$ and Py-L bands recorded after desorption at respectively 400 °C and 170 °C, were taken as a measure for the acid strength of the protonic and Lewis sites.

2.4. Catalytic tests

The catalytic tests were carried out in a 6-flow micro reactor using a fixed volume of catalyst (0.8 ml, corresponding to 65 mm of bed length) in down-flow 4 mm quartz reactors. To assure that the catalyst bed is located in the isothermal zone of the furnace, the reactors were loaded with quartz wool, 10 cm glass pearls (0.5 mm diameter), the catalyst, 10 cm glass pearls (0.5 mm diameter), and a second quartz wool plug. The glass pearls have limited conversion; less than 3% EB conversion under all applied conditions. The reactor gas feed is a mixture that can consist of CO_2, N_2, and air that counts for a gas-flow rate of 36 mL (STP).min^{-1}; the liquid EB-feed flow rate is 1 g/h (3.54 ml (STP).min^{-1} vapor) that is evaporated upstream each reactor in a α-Al_2O_3 column, resulting in a 1:9 molar ratio of ethylbenzene to gas (~10 *vol.* % EB). This corresponds with operation at a GHSV of 3000 l/l/h. The total pressure was 1.2-1.3 10^5 Pa. The

reactor exhaust gas was analyzed by gas chromatography using a combination of columns (0.3m Hayesep Q 80-100 mesh with back-flush, 25m × 0.53mm Porabond Q, 15 m×0.53mm molsieve 5A, and RTX-1 with 30m×0.53mm) with TCD and FID detectors. This configuration allows quantifying permanent gases such as CO_2, H_2, N_2, O_2, CO as well as hydrocarbons (methane, ethane, ethene, benzene, toluene, ethylbenzene, styrene, and heavy aromatics). The catalytic tests were carried out under practical conditions of 20 % excess O_2 with respect to the ODH reaction and a concentrated EB feed of 10%. The applied feed compositions were (*vol*.%): 9.8% EB, 5.9% O_2, 84.3% N_2 (for O_2:EB=0.6) and 9.8% EB, 1.9% O_2, 88.3% N_2 (for O_2:EB=0.2). If not stated otherwise, for all EB conversion data the oxygen conversion is complete. All physical characterizations for the spent catalysts were done after the complete testing cycle of 60 h. A more complete description of the testing protocol can be found elsewhere [80].

3. Results and discussion

3.1. Characterization of the fresh hybrid catalysts

The thermal stability and amount of organic material of the P-hybrids were determined by TGA (Fig. 1). The carbon contained in the hybrid starts to burn in air at around 450 °C with a maximum rate at 575 °C for both hybrids. The organic content as determined by TGA is 17.2 and 19.1 *wt.* %. The oxidation stability in air was compared to the conventional MWCNT and a P-free counterpart (15C/AS) using the oxidation rate profiles (TPO, Fig. 1). Most of the materials start to burn in air above 450 °C, but the maxima vary among them; the most stable is MWCNT with a maximum at 625 °C. The maxima of the P-promoted hybrids virtually coincide with the 15C/AS material, so apparently P has no effect on inhibiting the combustion of the deposited carbon. However, the determination of the apparent activation energies (AAE) will give a more thorough interpretation of the thermal stability, as it was shown in our previous study

[54]. Figure 2 shows the AAE for the combustion of the deposited carbon as determined by the Ozawa-Flynn-Wall model. A clear trend is seen where the P-based hybrids have an increased AAE of around 13% higher than that of the 15C/AS and lower than that of MWCNT (the latter is 24% higher than 15C/AS). Therefore, the AAE predicts a better thermal stability attributed to the P effect and possibly this will cause a stable operation under the reaction   conditions.

High oxygen content of the deposited carbon has been one of the crucial compositional features for the selective, and active, sites for the reaction-produced active coke in the EB ODH reaction [22]. The elemental composition of both 3P/15C/AS and 6P/15C/AS hybrids was determined by CHN and compared to reported values for ODH cokes (Fig. 3) [22,81]. The O:C ratios (0.10-0.15 at.) lie within the typical reported limits for ODH coke. Therefore, it can be expected that the FA-based hybrids will be readily active/selective for the ODH reaction. Studies about FA-based carbons, reports low O:C ratios (0.02-0.12)

[63,65,66,68]. Burket *et al*. [68] demonstrated that the O removal takes place during the collapse of the mesopores; thus the high O:C ratio in the 3P/15C/AS and 6P/15C/AS can be attributed to the stable mesopores (in both cases 96% of the total pore volumes are mesoporous) due to the presence of the mesoporous silica support underneath that prevents the carbon collapse.

Other relevant features are the porosity of the hybrid material in comparison to the fresh silica and the type of coke formed. The Raman spectra of both materials (3P/15C/AS and 6P/15C/AS) in Fig. 4) reveal two broad superimposing adsorptions centered at 1610 and 1375 cm^{-1}, which are characteristic of aromatic and amorphous carbon, G and D peaks, respectively [82,83].

Comparison of the gas adsorption N_2 isotherms was done in Figure 5. The shape of the isotherms does not change upon deposition of carbon and phosphorus; isotherms of type

14

IV with hysteresis Hl were observed as for the bare AS silica; representing solids with high pore size uniformity and facile pore connectivity [84,85]. No pore network effects were observed, indicating that the pores are well connected after the carbon/phosphorus addition. There is, however, a substantial reduction of the pore volume of 37% (3P/15C/AS) and 42% (6P/15C/AS); while the surface area only changes 8 and 18%, respectively (Table 1). The BJH pore size distribution in Figure 3 (inset) shows a decrease of the intensity, associated to the filling effect of the carbon. Calculation of the average geometrical pore size (Table 1) reveals a reduction of pore size from 15.8 nm (AS) to 10.9 nm (3P/15C/AS) and 11.3 nm (6P/15C/AS). The t-plot analysis evidences the formation of micropores that contribute in 3.8-3.9% of the total pore volume (Table S-2). Therefore, there are two opposing effects on the texture; significant reduction of mesopore volume (and pore size) and formation of micropore volume, that will overall result in a moderate reduction of the total surface area. This is because the created micropores contribute significantly more to the surface area than mesopores. Therefore, the overall interpretation of the textural data is that a P-containing carbon coating has been created with the shrinking of the existing mesopores and the formation of new micropores in the carbon; those will contribute in maintaining a moderately high surface area.

The acidity was evaluated by pyridine adsorption; the 1545 cm^{-1} band corresponds to pyridinium ions (PyH$^+$) on Brønsted sites and the 1445 cm^{-1} band to of coordinatively bonded pyridine to Lewis sites (PyL) (Figure 6, Table 1). For the reference sample 15C/AS no traces of Brønsted nor Lewis acid sites are detected. Small amounts of Lewis acid sites are discriminated for the P-containing hybrids. The acidity is much higher for the P/SiO$_2$ counterparts. The 3P/AS contains both Brønsted and Lewis sites, while the higher P-loading 6P/AS only Brønsted sites are detected. Py-thermodesorption studies evidenced that the acid sites of the highest strength was the most populated in 3P/AS,

15

i.e. with the highest A_{400}/A_{170} ratio, Table 1.

3.2. Pseudo-steady state EB ODH catalyst performance

The catalyst performances are summarized in Figures 7 to 10; EB conversion, selectivity to CO_x, selectivity to ST and ST yield are represented as a function of time-on-stream (TOS) at various temperatures and O_2:EB ratios. The selectivities to side products (not shown) are small and almost constant as a function of the reaction conditions; benzene and toluene are formed in low percent concentrations along with trace amounts of oxygenates. The selectivities to these byproducts do not substantially vary. The sum of ST and COx selectivities (Fig. 8 and 9) is on average above 96% of the converted ethylbenzene.

Figures 7-10 compare the P-hybrids with various types of relevant EB ODH catalysts under similar conditions. The P-hybrids are stable in terms of EB conversion and ST selectivity, though there is a slight gasification and burning process as reflected in the COx profiles (Fig. 9). It is noteworthy finding that the P-hybrids were stable for 60 h. In our previous work [54] we reported that the P-free hybrid (15C/AS) starts to decompose after 20 h with the complete disappearance of the introduced carbon and very low conversion (<2.5%) after 35 h, which is the result of the residual bare silica performance. Therefore, the addition of P has a remarkable effect on the thermal stability. This is consistent with the calculated apparent activation energies by the Ozawa-Flynn-Wall model that showed values for the P-hybrids (130-131 kJ.mol^{-1}) near the MWCNT (144 kJ.mol^{-1}) and higher than that for the 15C/AS (116 kJ/mol^{-1}). Thus the oxidation stability in air appears to correlate to the stability under the reaction conditions. However, as will be discussed later, there is another factor that contributes to the performance; the formed coke due to the presence of the observed acidic groups.

The performance of the P-hybrids is compared to state-of-the-art P/SiO$_2$, MWCNT, and

16

prior work on C/SiO_2 hybrids; the latter reported elsewhere [54]. The selectivity to ST ranges 85-90% (Fig. 8), which is high, but slightly lower when compared to the P/SiO_2 counterparts (85-95%) and much better than that of C/SiO_2 that ranged between 50 and 80% [54] under identical reactions conditions. A more competitive carbon-based catalyst would be a conventional commercially available cleaned MWCNT. There is an ample agreement that the reaction is catalysed by the coke formed on the acid sites (or available sites), containing oxygen groups. The temperature effect on the performance is a function of two factors; the rate constant with increasing temperature and the decrease in the number of active sites due to the thermolysis of oxygen containing groups at higher temperatures. This can be clearly seen in the performance of this MWCNT, where the optimal temperature was found at 450 °C, while at 475 °C the conversion decreases. This is consistent with Delgado *et al.* [32] and Zhao *et al.* [35], where a maximum conversion was observed at a certain temperature.

When the ST selectivity or EB conversion of these P-based hybrids is compared to the MWCNT, it can be seen that the P-hybrids behave much better. At high temperatures (450-475 °C) both conversion and selectivity are optimal for the P-hybrids, while the difference becomes negligible at lower temperature (425 °C). The trends in selectivity were opposing. While the selectivity of the MWCNT was best at lower temperatures (in agreement with literature that often reports an operation range between 350-400 °C), higher temperatures were most favourable for the P-hybrids. Thus the P-hybrids seem to be a high-temperature catalyst for this application with higher selectivity and conversion than that of a conventional MWCNT.

An additional feature to remark is that the P-hybrids are readily active and selective while the P-based silica catalysts (3P/AS and 6P/AS) require substantial time to reach the pseudo-stationary conversion (Fig. 7); 8 and 15 h respectively, under the applied conditions are required. This induction period is thought to be due to the slow formation

of active coke on the catalyst surface, induced by the acidity of the phosphates groups [10,21]. This deposited coke is readily selective since the selectivity profiles do not have such activation period (Fig. 8). The ST yield of these P/silica catalysts (Fig. 10) is determined by a complex activation-deactivation phenomena of the conversion, related to the unlimited coke build up process.

When comparing the performance at 450 °C between the second and last sequence in the catalytic test, it can be observed that the P-based hybrids drop in conversion; the conversion levels do not return to the values obtained in the second cycle but it declines. This can be associated to the on-going coking, though other deactivating phenomena associated to the silica itself cannot be ruled out. Such a drop in conversion is lower than those for MWCNT and P/SiO$_2$ catalysts, with the exception of 6P/AS that seems to be activating due to the slow coke deposition. When analysing the long-term reaction times, the P-hybrids performance tends to the 3P/SiO$_2$ catalyst in terms of conversion with a somewhat lower selectivity to styrene than the 6P/SiO$_2$ catalyst. Such type of comparison with a competitive catalyst is hardly found in the literature and it indicates that it seems to be hard finding a carbon-based catalyst that outperforms the conventional P/SiO$_2$.

In conclusion, the P-based hybrids show interesting features. They lack the induction period, *i.e.* they are readily active and selective, and the selectivity and conversion at high temperature (450-475 °C) is superior when compared to the MWCNT. The difference in selectivity and conversion becomes negligible when working at 425 °C. They seem to be thermally stable, with no major gasification or burning for 60 h under the applied reaction conditions. The on-going deactivation is less extensive than the other reference catalysts tested. In the long-term they behave like P/SiO$_2$ in terms of conversion with a lower ST selectivity.

3.2. Spent catalysts characterization and deactivation

The coke content in the spent catalysts was determined by TGA (Fig. S-1). The coke build-up was calculated by the difference between the organic content of the spent catalyst minus that of the starting catalyst. Figure 11 shows that the P-hybrids build up coke during the reaction to *ca.* +23-24 *wt.* %, while in a previous work it was shown that the P-free 15C/AS does not build any coke but the original carbon was fully gasified/combusted during the reaction [54]. Thus, P can stabilize the FA-based coating as predicted by the AAE, but it also builds up coke. The latter is attributed to the observed Lewis acidity; the acidity is small but the reaction temperature is high, so this is favorable to promote the ODH coke build-up. The P/silica also builds coke in a much wider range, from 14 (6P/AS) to 43 *wt.*% (3P/AS), which is related to the differences in the surface areas of the fresh catalysts, but not strictly proportional. It is also due to the fact the 6P/AS is still in the activation process, so not all the surface area (and pore volume) has been covered (loaded) by coke.

Chemical analysis proves a higher oxygen content of the spent hybrid catalysts than that of the fresh counterparts (Table S-1); it comes from the additional coke formed during the reaction that is richer in oxygen-containing groups. The higher O content is consistent with a more facile oxidation in air, evidenced by a shift towards lower temperatures in the TGA maxima (Fig. 1). Representation of the composition in a van Krevelen-like plot (Fig.3) shows significant changes; higher O:C ratios and the C:H varies from a relatively high ratio, characteristic of FA-based carbons having low H content [63,65,66,68], to lower ratios near the values often reported for the ODH coke. It is obvious that the fresh hybrid catalysts cannot be hydrogenated under the ODH conditions; hence this compositional effect is ascribed to the deposition during the reaction of new ODH coke that is richer in H and O.

Raman spectra of the spent hybrid catalysts indicate the presence of a more ordered

structure that has been formed during the reaction. The D/G peak ratio becomes smaller (Fig. 4 and Table S-4) and this can be explained by two effects: 1) removal of the (more) amorphous carbon domains by gasification/burning and 2) deposition of sp^2-rich carbon materials, or both effects simultaneously; the second is due to the buildup of new poly-aromatic ODH coke.

Therefore, TGA/TPO, CHN, and Raman reveal the formation of a coke with different nature than that of the starting P-hybrid.

Porosity evaluation of the spent hybrids evidences that a reduction of the surface area and pore blockage are the main sources of catalyst modification during reaction. The specific surface area and pore volume are reduced around 70-80% for both parameters (Table 1), resulting in a less active catalytic system. The isotherms change the shape having a closure point around 0.45 in the relative pressure (Fig. 12), indicating the presence of pore network restrictions associated to the over-coking from the reaction. The spent 3P/AS and 6P/AS also manifested a substantial reduction of surface area (63 and 24%) and pore volume (80 and 43%) (Table 1, Fig. 12); the 3P/AS has pore network effects, while 6P/AS does not have it because it has much larger pores and less deposited coke. The 6P/AS is also less affected possibly because the surface is not yet fully covered in coke; the conversion keeps increasing after 55 h, which is an indication of on-going coke build-up. Thus, over-coking is identified as responsible for the decrease in the texture for both P/silica and P/C/silica hybrids during reaction.

It was found that the deactivation is very weak (when comparing the EB conversion at 450 °C between the second and last sequence in the catalytic test) despite the surface area drops about 70-75%. This is due to the presence of mesopores pores; the pore sizes were always > 9 nm. This is consistent with Pereira *et al.* [28] for their carbons study, where the EB conversion was not much affected by the surface area for pores above 1.2

nm.

4. Conclusions

The thermal stability of a composite material derived from the polymerization and pyrolysis of furfuryl alcohol on a commercial silica, can be enhanced by P addition. This is concluded from the estimation of the apparent activation energies in air oxidation. These P-modified hybrids are readily active, selective and indeed stable in the applied reactions conditions, in line with the apparent activation energies. At high temperatures (450-475 °C) they perform better than a conventional MWCNT while the difference becomes negligible at lower temperature. Introduced acidity by the P-addition is responsible for the coke build-up, which gives rise to a decrease of the surface area and pore volume during reaction. Comparison with a reference P/SiO_2 counterparts indicates a very similar yield than the hybrids but more selective to ST for P/SiO_2. In the long term operation, the (optimal) P/SiO_2 appears to be a better choice in terms of selectivity. The benefit of the P-hybrid is the lack of the induction period since the introduced carbon is readily active and selective for the EB ODH reaction.

References

[1] R.A. Meyers, Handbook of petrochemicals production processes, McGraw-Hill, New York, 2005.

[2] F. Cavani, F. Trifiro, Appl. Catal. A: Gen. 133 (1995) 219–239.

[3] A.I. Kozharov, L.A. Makhlis, A.E. Lisovskii, T.G Alkhazov, B.E. Vasserberg, Rus. Chem. Bul. 26 (1977) 477-480.

[4] Y. Iwasawa, H. Nobe, S. Ogasawara, J. Catal. 31 (1973) 444-449.

[5] T.G Alkhazov, A.E. Lisovskii, Kinet. Catal. 17 (1976) 375-379.

[6] C. Nederlof, F. Kapteijn, M. Makkee, Appl. Catal. A: Gen. 417 (2012) 163-173.

[7] C. Nederlof, V. Zarubina, I.V. Melián-Cabrera, H.J. Heeres, F. Kapteijn, M. Makkee, Catal. Sci. Technol. 3 (2013) 519-526.

[8] V. Zarubina, C. Nederlof, B. Van der Linden, F. Kapteijn, H.J. Heeres, M. Makkee, I.V. Melián-Cabrera, J. Mol. Catal. A: Chem. 381 (2014) 179-187.

[9] G. Emig, H. Hofmann, J. Catal. 84 (1983) 15-26.

[10] G.E. Vrieland, J. Catal. 111 (1988) 1-13.

[11] G.E. Vrieland, H.R. Friedli, Method of oxydehydrogenation of ethyl benzene. United States Patent 3,933,932 (1976).

[12] F. M. Bautista, J.M. Campelo, D. Luna, J.M. Marinas, R.A. Quirós, A.A. Romero, Appl. Catal. B: Environ. 70 (2007) 611-620.

[13] Y. Murakamo, K. Iwayama, H. Uchida, T. Hattori, T. Tagawa, J. Catal. 71 (1981) 257-269.

[14] Y. Murakamo, K. Iwayama, H. Uchida, T. Hattori, T. Tagawa, Appl. Catal. 2 (1982) 67-74.

[15] A. Schraut, G. Emig, H.G. Sockel, Appl. Catal. 29 (1987) 311-326.

[16] G. Bagnasco G, P. Ciambelli, M. Turco, A. La Ginestra, P. Patron, Appl. Catal. 68 (1991) 69-79.

[17] L.A. Arrúa, D.E. Ardissone, O.D. Quiroga, J.B. Rivarola, React. Kinet. Catal. Lett. 56 (1995) 383-389.

[18] Z. Dziewiecki, M. Jagiello, A. Makowski, React. Funct. Polym. 33 (1997) 185-191.

[19] G.E. Vrieland, H.R. Friedli, Oxydehydrogenation of ethyl benzene. United States Patent 3,923,916 (1975).

[20] H. Hofmann, G. Emig, W. Ruppert, Process for preparing styrene, and an appropriate agent. United States Patent 4,400,568 (1983).

[21] D.B. Tagiyev, G.O. Gasimov, M.I. Rustamov, Catal. Today. 102 (2005) 197-202.

[22] A.E. Lisovskii, C. Aharoni, Catal. Rev. Sci. Eng. 36 (1994) 25–74, and references therein.

[23] T.G. Alkhazov, A.E. Lisovskii, T.Kh. Guiakhmedova, React. Kinet. Catal. Lett. 12 (1979) 189-193.

[24] G.C. Grunewald, R.S. Drago, J. Mol. Catal. 58 (1990) 227-233.

[25] M.F.R Pereira, J.J.M. Orfão, J.L. Figueiredo, Appl Catal A-Gen. 184 (1999) 153-160.

[26] M.F.R. Pereira, J.J.M. Orfão, J.L. Figueiredo, Appl. Catal. A: Gen. 196 (2000) 43-54.

[27] M.F.R. Pereira, J.J.M. Orfão, J.L. Figueiredo, Appl. Catal. A: Gen. 218 (2001) 307-318.

[28] M.F.R. Pereira, J.J.M. Orfão, J.L. Figueiredo, Colloid Surface A. 241 (2004) 165-171.

[29] A. Guerrero-Ruiz, F. Rodriguez-Reinoso, Carbon 32 (1994) 23-29.

[30] G. Mestl, N.I. Maksimova, N. Keller, V.V. Roddatis, R. Schlögl, Angew. Chem. Int. Ed. 40 (2001) 2066-2068.

[31] M.F.R. Pereira, J.J.M. Orfão, J.L. Figueiredo, Carbon 40 (2002) 2393-2401.

[32] J.J. Delgado, R. Vieira, G. Rebmann, D.S. Su, N. Keller, M.J. Ledoux, R. Schlögl, Carbon 44 (2006) 809–812.

[33] J.J. Delgado, D.S. Su, G. Rebmann, N. Keller, A. Gajovic, R. Schlögl, J. Catal. 244 (2006) 126–129.

[34] P. Li, T. Li, J.H. Zhou, Z.J. Sui, Y.C. Dai, W.K. Yuan, D. Chen, Micropor. Mesopor. Mat. 95 (2006) 1-7.

[35] T.J. Zhao, W.Z. Sun, X.Y. Gu, M. Rønning, D. Chen, Y.C. Dai, W.K. Yuan, A. Holmen, Appl. Catal. A: Gen. 323 (2007) 135-146.

[36] N. Keller, N.I. Maksimova, V.V. Roddatis, M. Schur, G. Mestl, Y.V. Butenko, V.L. Kuznetsov, R. Schlogl, Angew. Chem. Int. Ed. 41 (2002) 1885–1888.

[37] D.S. Su, N.I. Maksimova, G. Mestl, V.L. Kuznetsov, V. Keller, R. Schlogl, N. Keller, Carbon 45 (2007) 2145–2151.

[38] M.F.R. Pereira, J.L. Figueiredo, J.J.M. Orfão, P. Serp, P. Kalck, Y. Kihn, Carbon 42 (2004) 2807-2813.

[39] H.Y. Liu, J.Y. Diao, Q. Wang, S.Y. Gu, T. Chen, C. Miao, W. Yang, D.S. Su, Chem. Commun. 50 (2014) 7810-7812.

[40] Z.K. Zhao, W.Z. Li, Y.T. Dai, G.F. Ge, X.W. Guo, G.R. Wang, ACS Sus. Chem. Eng. 3 (2015) 3355.

[41] H. Ba, Y. Liu, X. Mu, W.-H. Doh, J.-M. Nhut, P. Granger, C. Pham-Huu, Appl. Catal. A. 499 (2015) 217.

[42] H. Ba, L. Truong-Phuoc, Y. Liu, C. Duong-Viet, J.-M. Nhut, L. Nguyen-Dinh, P. Granger, C. Pham-Huu, Carbon 96 (2016) 1060.

[43] J. Diao, H. Liu, Z. Feng, Y. Zhang, T. Chen, C. Miao, W. Yang, D.S. Su, Catal. Sci. Technol., 5 (2015) 4950-4953.

[44] H. Ba, L. Truong-Phuoc, Y. Liu, C. Duong-Viet, J.-M. Nhut, L. Nguyen-Dinh, P. Granger, C. Pham-Huu, Carbon 96 (2016) 1060.

[45] D.S. Su, N. Maksimova, J.J. Delgado, N. Keller, G. Mestl, M.J. Ledoux, R. Schlögl, Catal. Today 102 (2005) 110–114.

[46] J. Zhang, D. Su, A. Zhang, D. Wang, R. Schlögl, C. Hebert, Angew. Chem. Int. Ed. 46 (2007) 7319-7323.

[47] B. Nigrovski, P. Scholz, T. Krech, N.V. Qui, K. Pollok, T. Keller, B. Ondruschka, Catal. Commun. 10 (2009) 1473-1477.

[48] N.V. Qui, P. Scholz, T. Krech, T.F. Keller, K. Pollok, B. Ondruschka, Catal. Commun. 12 (2011) 464-469.

[49] Z. Zhao, Y. Dai, G. Ge, X. Guo, G. Wang, Green Chem. 17 (2015) 3723.

[50] J. Gläsel, J. Diao, Z. Feng, M. Hilgart, T. Wolker, D.S. Su, B.J.M. Etzold, Chem. Mater. 27 (2015) 5719.

[51] J. Diao, H. Liu, J. Wang, Z. Feng, T. Chen, C. Miao, W. Yang, D.S. Su, Chem. Commun. 51 (2015) 3423.

[52] J. Zhang, D.S. Su, R. Blume, R. Schlögl, R. Wang, X. Yang, A. Gajović, Angew. Chem. Int. Ed. 49 (2010) 8640-8644.

[53] J.J. Delgado, X. Chen, J.P. Tessonnier, M.E. Schuster, E. Del Rio, R. Schlögl R, D. Su, Catal Today 150 (2010) 49-54.

[54] V. Zarubina, H. Talebi, C. Nederlof, F. Kapteijn, M. Makkee, I. Melián-Cabrera, Carbon 77 (2014) 329-340.

[55] D.W. McKee, Carbon 10 (1972) 491-497.

[56] D.W. McKee, C.L Spiro, E.J. Lamby, Carbon 22 (1984) 285-290.

[57] Y.J. Lee, L.R. Radovic, Carbon 41 (2003) 1987-1997.

[58] B. Frank, A. Rinaldi, R. Blume, R. Schlögl, D.S. Su, Chem. Mater. 22 (2010) 4462-4470.

[59] B. Frank, J. Zhang, R. Blume, R. Schlögl, D.S. Su, Angew. Chem. Int. Ed. 48 (2009) 6913-6917.

[60] W.B. Innes, Anal Chem. 28 (1956) 332-334.

[61] H. Eckert, Y.A. Levendis, R.C. Flagant, J. Phys. Chem. 92 (1988) 5011-5009.

[62] D.S. Lafyatis, J. Tung, H.C. Foley, Ind. Eng. Chem. Res. 30 (1991) 865-873.

[63] A. Shindo, K. Izumino, Carbon 32 (1994) 1233-1243.

[64] H.C. Foley, Micropor. Mesopor. Mat. 4 (1995) 407-433.

[65] Z. Wang, Z. Lu, X. Huang, R. Xue, L. Chen, Carbon 36 (1998) 51-59.

[66] A.J.G. Zarbin, R. Bertholdo, M.A.F.C. Oliveira, Carbon 40 (2002) 2413-2422.

[67] J. Yao, H. Wang, J. Liu, K.Yu. Chan, L. Zhang, N. Xu, Carbon 43 (2005) 1709-1715.

[68] C.L. Burket, R. Rajagopalan, A.P. Marencic, K. Dronvajjala, H.C. Foley, Carbon 44 (2006) 2957-2963.

[69] H. Wang, J. Yao, Ind. Eng. Chem. Res. 45 (2006) 6393-6404.

[70] L. Radhakrishnan, J. Reboul, S. Furukawa, P. Srinivasu, S. Kitagawa, Y. Yamauchi, Chem. Mater. 23 (2011) 1225-1231.

[71] M. Kruk, M. Jaroniec, R. Ryoo, S.H. Joo, J. Phys. Chem. B. 104 (2000) 7960-7968.

[72] M. Kruk, M. Jaroniec, T.W. Kim, R. Ryoo, Chem. Mater. 15 (2003) 2815-2823.

[73] D.P. Serrano, J.A. Botas, P. Pizarro, R. Guil-Lopez, G. Gomez, Chem. Commun. 48 (2008) 6585-6587.

[74] G. Busca, G. Ramis, V. Lorenzelli, P.F. Rossi, A. Laginestra, P. Patrono, Langmuir 5 (1989) 911.

[75] S. Brunauer, P.H. Emmett, E. Teller, J. Am. Chem. Soc. 60 (1938) 309-319.

[76] E.P. Barrett, L.G. Joyner, P.H. Halenda, J. Am. Chem. Soc. 73 (1951) 373-380.

[77] B.C. Lippens, J.H. De Boer, J. Catal. 4 (1965) 319.

[78] T. Hatakeyama, L. Zhenhai, Handbook of Thermal Analysis, John Wiley & Sons Ltd., Chichester, 1998.

[79] K. Góra-Marek, M. Derewiński, J. Datka, P. Sarv, Catal. Today 101 (2005) 131-138.

[80] C. Nederlof, PhD Thesis, Delft University of Technology, 2012.

[81] R. Fiedorow, W. Przystajko, M. Sopa, J. Catal. 68 (1981) 33–41.

[82] Z. Wang, Z. Lu, X. Huang, R. Xue, L. Chen, Carbon 36 (1998) 51-59.

[83] S. Bertarione, F. Bonino, F. Cesano, A. Damin, D. Scarano, A. Zecchina, J. Phys. Chem. B. 112 (2008) 2580-2589.

[84] K.S.W. Sing, D.H. Everett, R.A.W. Haul, L. Moscou, R. Pierotti, J. Rouquerol, T. Siemieniewska, Pure Appl. Chem. 57 (1985) 603-619.

[85] M. Kruk, M. Jaroniec, Chem. Mater. 13 (2001) 3169-3183.
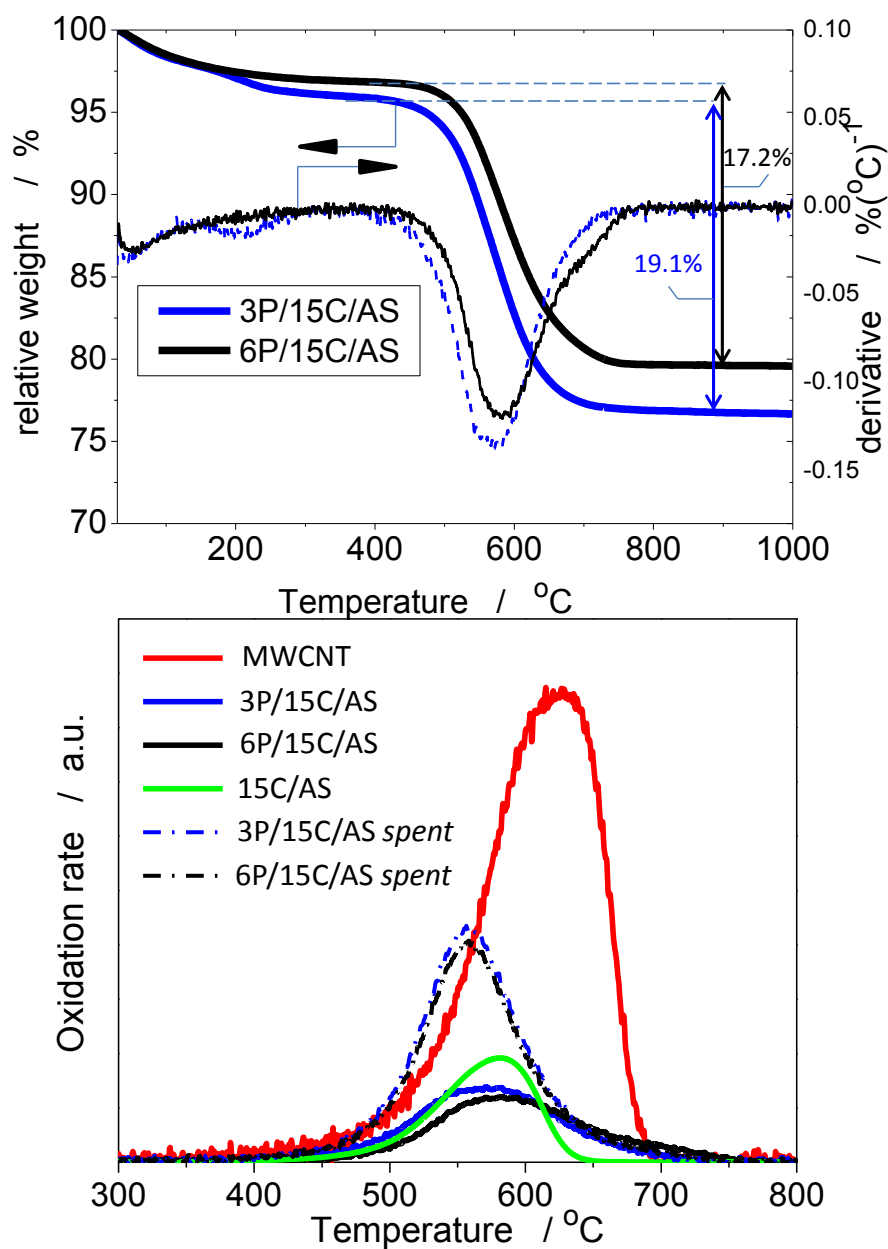
Figure 1. **Top)** TGA patterns of the fresh hybrids: 3P/15C/AS and 6P/15C/AS. Conditions 100 ml.min^{-1}, synthetic air, heating rate of 10 °C.min^{-1}. **Bottom)** Oxidation rate patterns (TPO) in air (10 °C.min^{-1}) for MWCNT, 3P/15C/AS, 6P/15C/AS, 15C/AS, spent 3P/15C/AS, and spent 6P/15C/AS. Conditions: synthetic air, 100 ml.min^{-1}, heating rate of 10 °C.min^{-1}. Typical sample amount ranged 5-8 mg.
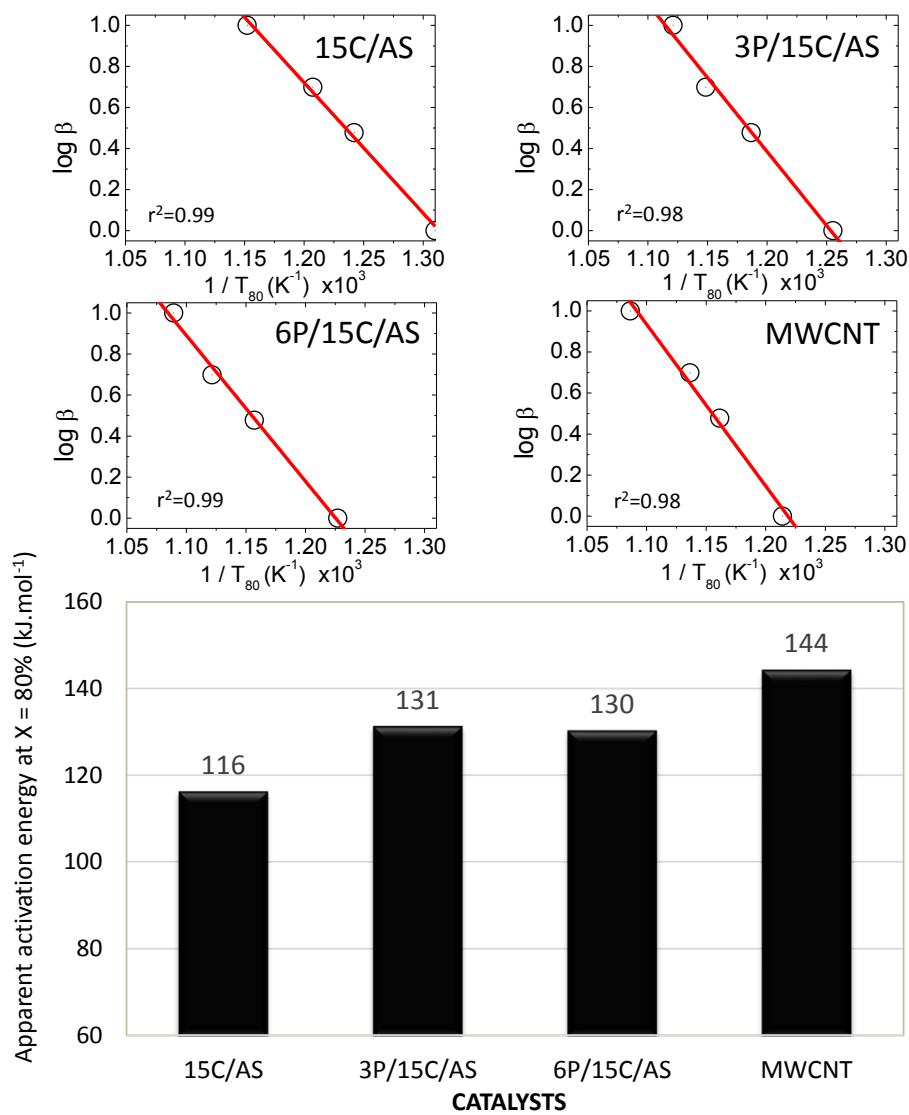
Figure 2. **Top)** Ozawa-Flynn-Wall (OFW) linearizations for the carbon combustion at 80% conversion; the value of the correlation coefficients is indicated (r^2). **Bottom)** derived OFW apparent activation energies (kJ.mol^{-1}).
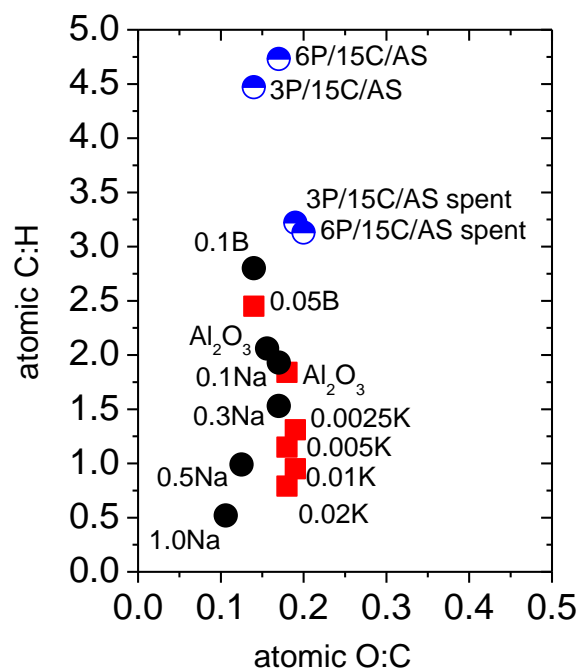
Figure 3. Van Krevelen-like plot representing the composition of the hybrids (◓): (3P/15C/AS and 6P/15C/AS), fresh and spent, in comparison with prior work, adapted from [●,81] and [■,22]. Raw data are given in Table S-1.
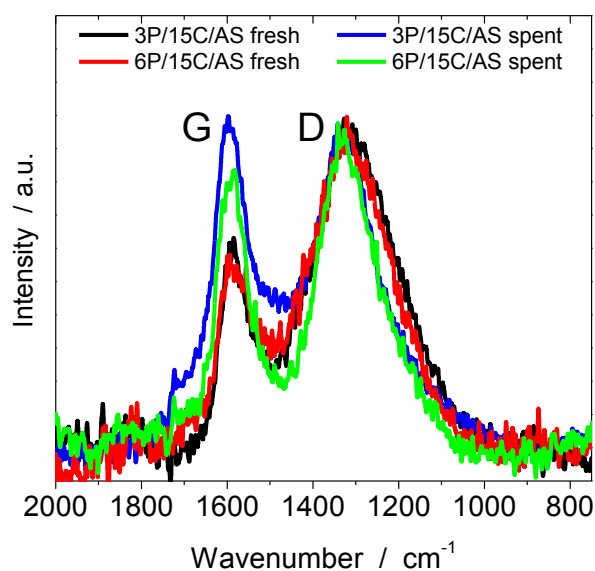
Figure 4. Raman spectra for the **fresh** and **spent** 3P/15C/AS and 6P/15C/AS catalysts.
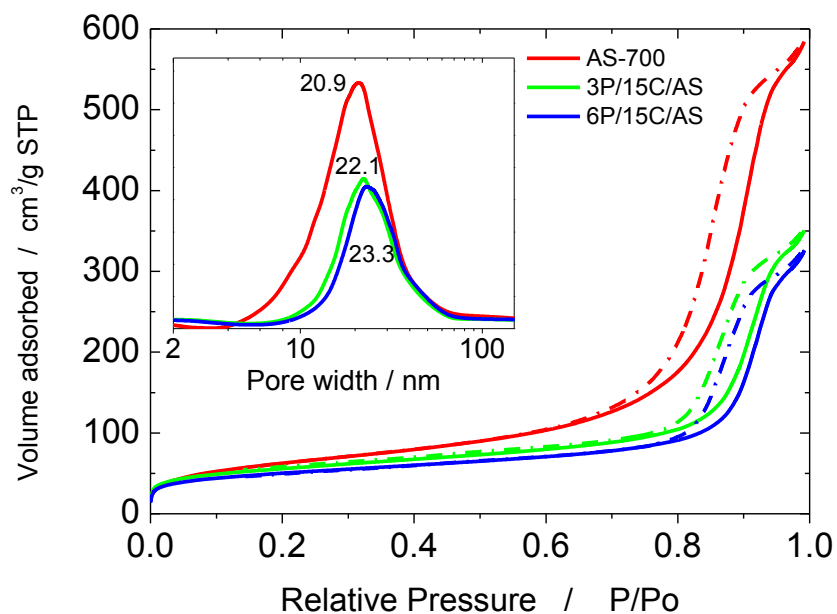
**Figure 5**. Nitrogen sorption isotherms at −196 °C for AS-700, 3P/15C/AS and 6P/15C/AS.

Inset: BJH pore size distribution of the adsorption data.
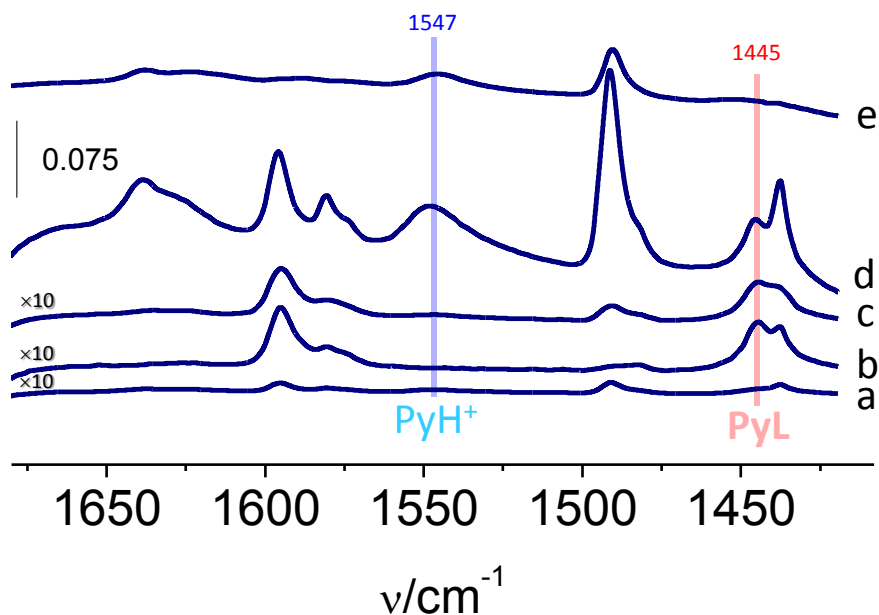
Figure 6. Qualitative IR spectra of adsorbed pyridine at 170 °C for **a)** 15C/AS, **b)** 3P/15C/AS, **c)** 6P/15C/AS, **d)** 3P/AS and **e)** 6P/AS.
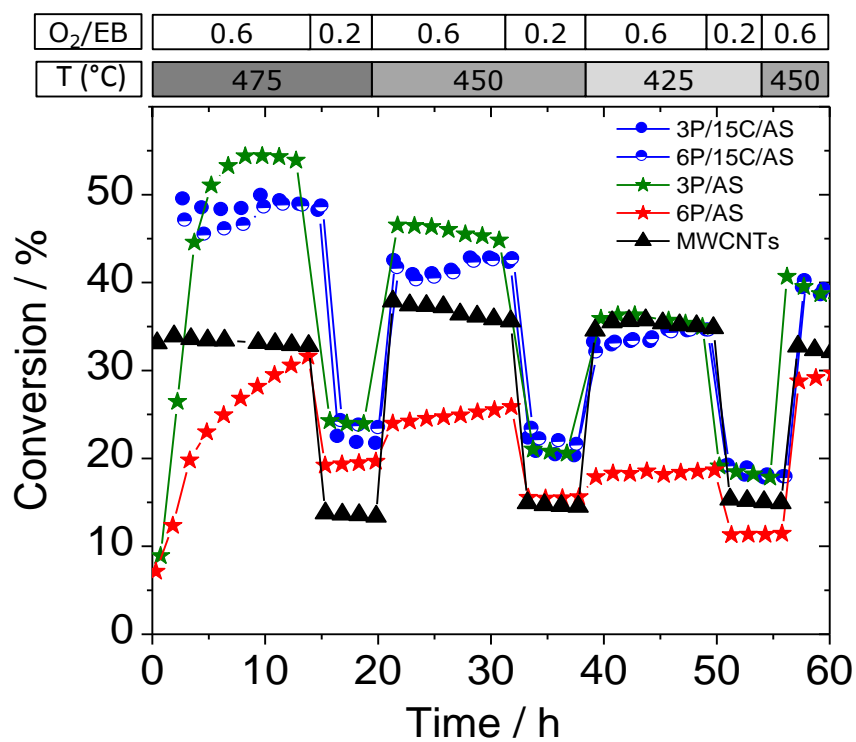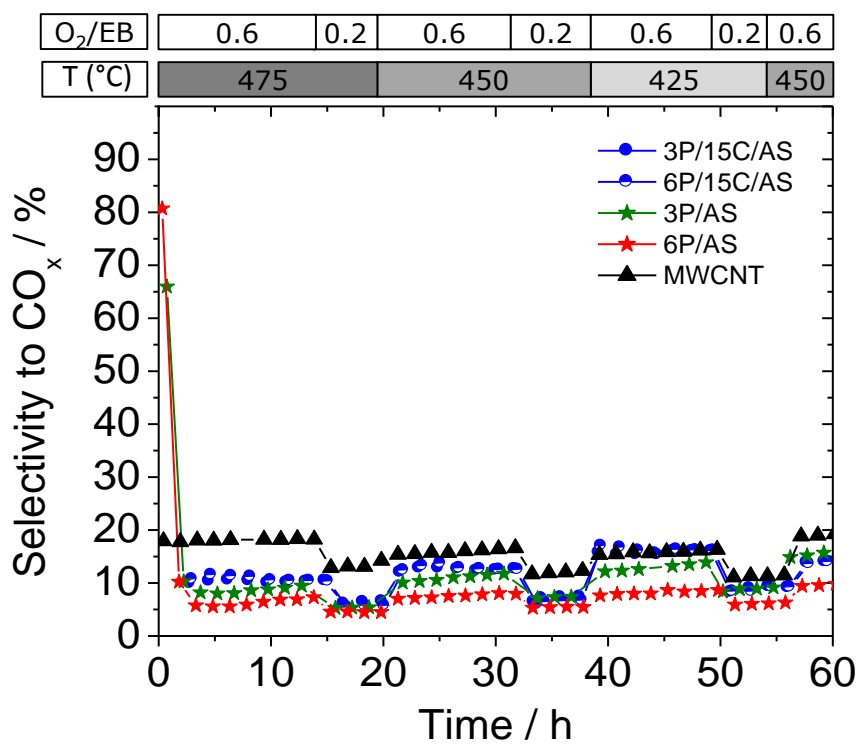
Figure 7. Time on stream ethylbenzene (EB) conversion at various temperatures (475, 450, 425, and 450 °C) and O_2/EB= 0.6 and 0.2 (*vol*); GHSV of 3000 l/l/h. Note that 3P/15C/AS and 6P/15C/AS overlaps for TOS > 20 h.
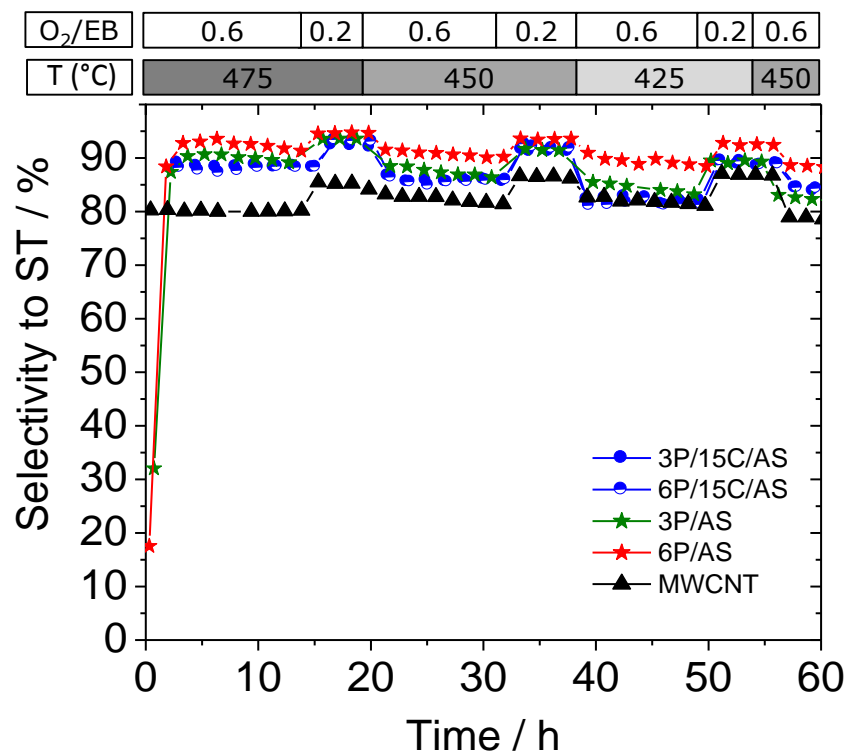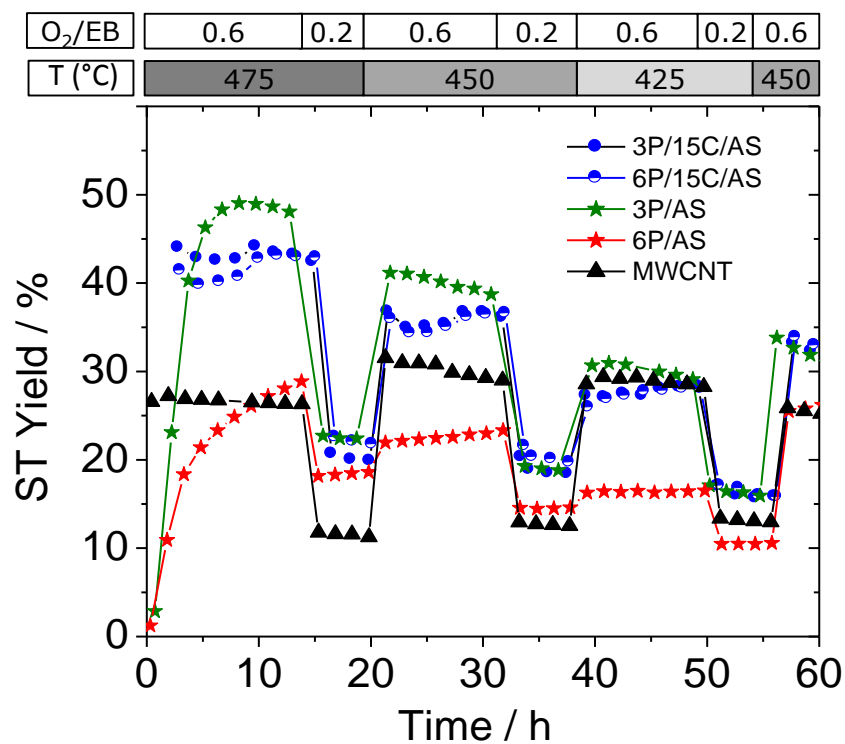
Figure 8. Time on stream selectivity to styrene (ST) at various temperatures (475, 450, 425, and 450 °C) and O_2/EB= 0.6 and 0.2 (*vol*); GHSV of 3000 l/l/h. Note that 3P/15C/AS and 6P/15C/AS overlaps for TOS > 20 h.

Figure 9. Time on stream selectivity to partial and total oxidation products, CO/CO$_2$ (COx) (**c**), and ST yield (**d**) at various temperatures (475, 450, 425, and 450 ^{o}C) and O$_2$/EB= 0.6 and 0.2 (*vol*); GHSV of 3000 l/l/h. Note that 3P/15C/AS and 6P/15C/AS overlaps for TOS > 20 h.

Figure 10. Time on styrene (ST) yield at various temperatures (475, 450, 425, and 450 $^\circ$C) and O$_2$/EB= 0.6 and 0.2 (*vol*); GHSV of 3000 l/l/h. Note that 3P/15C/AS and 6P/15C/AS overlaps for TOS > 20 h.
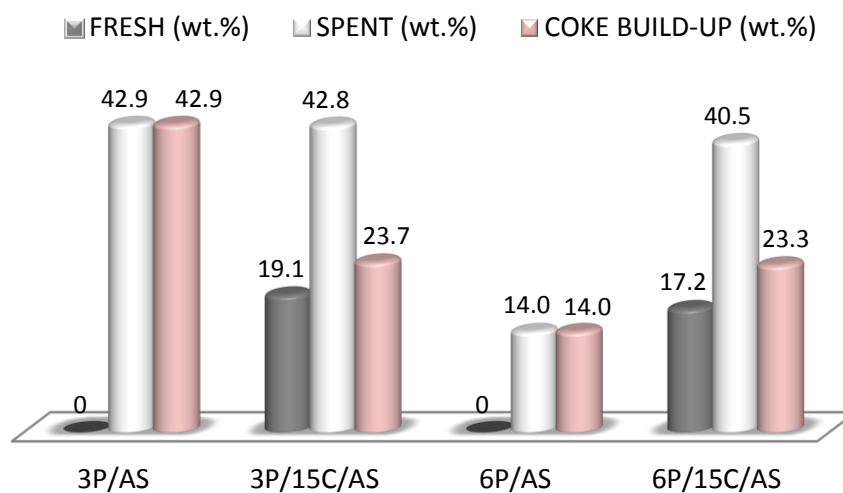
Figure 11. Organic contents for the fresh and spent catalysts after reaction. Coke build-up is defined as the difference spent minus fresh case. Raw data are given in Table S-3 and TGA patterns in Fig. 1-top and Fig. S-1.
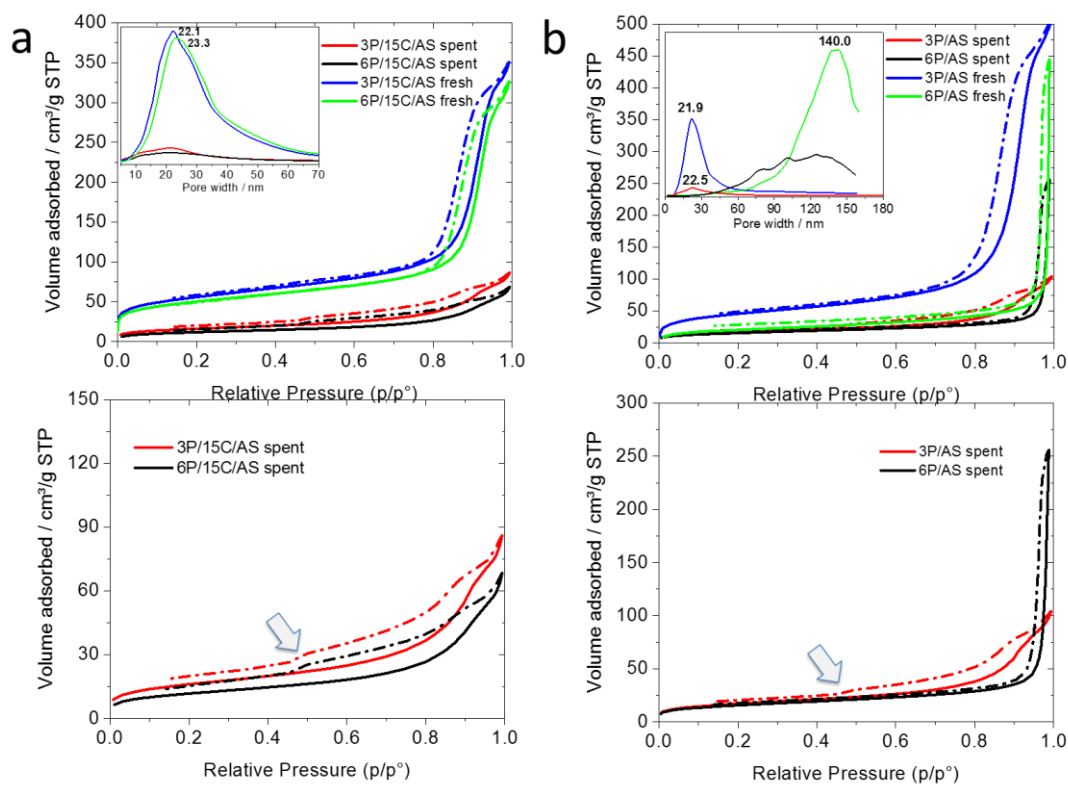
Figure 12. **A) Top)** Nitrogen sorption isotherms of the 3P/15C/AS and 6P/15C/AS, spent and fresh catalysts. Inset: BJH pore size distribution. **Bottom)** Zoom-in of the spent catalysts isotherms. **B) Top)** Data for the 3P/AS and 6P/AS, spent and fresh catalysts. Inset: BJH pore size distribution. **Bottom)** Zoom-in of the spent catalysts isotherms. The arrows indicate the low-pressure closure point at *ca.* 0.45 P/Po in the desorption step. Solid line: adsorption step; dashed line: desorption step.

Table 1. Textural parameters derived from N_2 adsorption at -196 °C and acidic properties of chosen materials (concentration and strength) derived from quantitative IR studies of Py sorption.

Material	S_{BET} (m^2.g^{-1})	V_T (cm^3.g^{-1})^{a,c}	Φ_{BJH} (nm)^d	Brønsted (µmol/g)	Brønsted A_{400}/A_{170}	Lewis (µmol/g)	Lewis A_{400}/A_{170}
AS *bare*	213	0.842	20.8 (15.8)	ND [e]	ND	ND	ND
3P/15C/AS	195 (−8)^b	0.532 (−37)^b	22.1 (10.9)	0	0	10	0
3P/15C/AS *spent*	58 (−70)^a	0.128 (−76)^a	*broad* (8.8)	ND	ND	ND	ND
6P/15C/AS	174 (−18)^b	0.492 (−42)^b	23.3 (11.3)	0	0	15	0.1
6P/15C/AS *spent*	42 (−76)^a	0.101 (−79)^a	*broad* (9.6)	ND	ND	ND	ND
MWCNT	406	1.100	3, 30.8	ND	ND	ND	ND
3P/AS	165	0.765	21.9 (18.5)	200	0.35	380	0.50
3P/AS spent	61 (−63)^a	0.155 (−80)^a	22.5 (10.1)	ND	ND	ND	ND
6P/AS	74	0.682	140 (36.9)	60	0.15	0	0
6P/AS spent	56 (−24)^a	0.392 (−43)^a	*broad* (28.0)	ND	ND	ND	ND
AC	959	0.609	*broad*	ND	ND	ND	ND

a. Value in parenthesis is the % of reduction with respect to the fresh material; **b.** % of reduction with respect to the AS *bare*; **c.** gas adsorption or internal pore volume; **d.** values in parenthesis are the average geometrical pore size as $4.10^3 V_T/S_{BET}$, **e.** not determined.